

Terahertz coherent transients from methyl chloride vapor

H. Harde

Universitaet der Bundeswehr, Holstenhofweg 85, 22043 Hamburg, Germany

N. Katzenellenbogen* and D. Grischkowsky*

IBM Watson Research Center, P.O. Box 218, Yorktown Heights, New York 10598

Received September 14, 1993; revised manuscript received December 17, 1993

A newly developed optoelectronic source for generating well-collimated beams of subpicosecond pulses of terahertz radiation was used to study coherent propagation effects in a spectrally thick medium of methyl chloride vapor. After the passage of the excitation pulse, we observe the subsequent emission of a coherent terahertz pulse train in the free-induction decay of the molecular vapor. The individual pulses of the train are separated by 38 ps, corresponding to the frequency separation between adjacent rotational lines of the excited manifold of more than 70 transitions. An analysis of the data determines the rotational constants and anharmonicity factors of the two naturally abundant methyl chloride isotopes. From the decay and reshaping of the pulse train the coherence relaxation time T_2 is obtained as a function of vapor pressure. Our observations indicate a strong nonmonotonic collision broadening and a van Vleck-Weisskopf line shape of the individual rotational lines.

1. INTRODUCTION

The experimental and theoretical study of coherent transient effects resulting from the interaction of electromagnetic radiation with resonant systems^{1,2} was recently extended to the terahertz frequency range.^{3,4} These experiments were based on exciting molecular vapors with freely propagating subpicosecond pulses of terahertz radiation and detecting the free-induction decay (FID) re-radiated by the vapors. This newly accessible frequency range, midway between the frequencies used for spin resonance and those of infrared and optical studies, is important both because of the samples that can be investigated and because of the unusual experimental conditions encountered with subpicosecond pulses of terahertz radiation. The recently developed optoelectronic terahertz-beam system used in these experiments produces well-collimated beams of subpicosecond pulses of freely propagating terahertz radiation.⁵⁻⁹ These pulses of terahertz electromagnetic radiation can be detected with signal-to-noise ratios of better than 10,000. Compared with studies of coherence effects in the radio frequency and the microwave regimes for nuclear- and electron-spin systems, the terahertz experiments involved samples that were of many wavelengths in length, so that in addition to the point response, propagation effects were also important. In contrast to investigations at infrared and optical frequencies, in which coherent transients are detected only as pulse intensities or as beat notes on a carrier,¹⁰⁻¹² the terahertz experiments directly measure the actual electric field of the transmitted radiation pulse and that radiated by the coherent response of the sample. This feature allows for experimental studies with unprecedented precision, and both the amplitude and the phase are measured within the broad bandwidth of the terahertz pulse extending from low frequencies up to 5 THz.

In this paper we extend the terahertz coherence stud-

ies to methyl chloride, which is a symmetric top molecule with a large electric dipole moment. This molecule is an interesting candidate for observation of coherent propagation effects under extreme conditions for which the vapor is an optically dense sample for the terahertz radiation. Owing to the high sensitivity and the excellent signal-to-noise ratio of the measuring system, additional molecular information can be obtained. Our measurements indicate that the individual rotational transitions have van Vleck-Weisskopf line shapes, with a strong nonmonotonic J dependence for the collision-broadening coefficient.

The propagation of a terahertz excitation pulse through methyl chloride vapor simultaneously excites a manifold of rotational transitions, thereby causing the molecules to radiate a FID signal consisting of a series of uniformly spaced subpicosecond terahertz pulses.^{3,4} For a similar phenomenon of infrared pulses emitted after excitation, see Refs. 13-16. Since the methyl chloride molecule is distinguished by absorption lines with an almost constant frequency spacing, after the initial excitation a periodic rephasing and dephasing of the entire ensemble of more than 70 excited transitions occurs during the FID and is manifest as a train of subpicosecond terahertz pulses with a repetition rate equal to the frequency separation between adjacent lines. This situation is quite similar to the mode locking of lasers. A coherent signal radiated by dipoles coming into phase and forming a macroscopic dipole moment is known from spin and photon echoes. Because of this and the fact that the frequencies are numerical multiples of the difference frequency between two lines, we term the periodic pulses terahertz commensurate echoes.³

These echoes carry almost complete information about the molecular system. From their temporal separation and pulse shapes we obtain the parameters of the molecule, and from their decay the coherence relaxation time

T_2 determined only by collisions. Doppler dephasing is completely negligible in this frequency range. We have measured, with a time resolution of better than 0.2 ps, trains of echoes extending to beyond 300 ps. These measurements are compared with theoretical simulations that we obtain by solving the wave equation for the propagation of the terahertz pulses through the vapor. The extremely low power of the terahertz excitation pulses permits the use of the linear dispersion theory in these calculations. In our analysis the linear response of the molecules to the propagating terahertz pulses was obtained in the frequency domain, and from the resulting spectral response the time-domain behavior was determined. A fit of the calculated pulse structure to the measurements determined the rotational constants and anharmonicity factors of the two naturally abundant methyl chloride isotopes. Furthermore, the collisional linewidth broadening was evaluated as a function of vapor pressure up to values for which the absorption lines are already completely overlapping. Owing to the high signal-to-noise ratio and the exceptional time resolution, the line shape and the strong variation of the pressure-broadened linewidths over the rotational spectrum were obtained.

2. EXPERIMENTAL SETUP

The high-performance optoelectronic source¹⁷ used to generate pulses of freely propagating terahertz electromagnetic radiation is shown in Fig. 1(a). The simple coplanar transmission line structure of the source chip consists of two 10- μm -wide metal lines separated by 80 μm fabricated on high-resistivity GaAs. Irradiating the metal-semiconductor interface (edge) of the positively biased line with focused ultrafast laser pulses produces synchronous bursts of terahertz radiation. This occurs because each laser pulse creates a spot of photocarriers in a region of extremely high electric field.¹⁸ The consequent acceleration of the carriers generates the burst of radiation. A colliding-pulse mode-locked dye laser provides the 623-nm, 60-fs excitation pulses at a 100-MHz repetition rate in a beam with an average power of 5 mW at the 10- μm -diameter excitation spot. The major fraction of the laser-generated burst of terahertz radiation is emitted into the GaAs substrate in a cone normal to the interface and is then collected and collimated by a crystalline silicon lens attached to the back side of the chip.

The terahertz optical components^{8,9} used in the complete optoelectronic system are illustrated in Fig. 1(b) and consist of two matched crystalline silicon lenses, one in contact with the back side of the GaAs source chip and the other with the silicon-on-sapphire detection chip. Each lens is located near the foci of two identical paraboloidal mirrors. The combination of the silicon lens and the paraboloidal mirror collimates the emitted radiation to beam diameters proportional to the wavelength and with a frequency-independent divergence typically of 25 mrad. The second identical combination on the receiving end focuses the terahertz beam onto the detector. The vapor cell containing the sample under investigation is also indicated. The cell is constructed of stainless steel, and, to reduce the complicating effects of multiple reflections from the cell windows, 2-cm-thick, 5-

cm-diameter, high-resistivity (10 k Ω cm) silicon windows are used. Silicon is an ideal window material because of its almost complete transparency and lack of dispersion in the terahertz frequency range.⁸ The length of the vapor path is 22.5 cm, and the cell has a clear aperture 4 cm in diameter. The entire system is located in an airtight enclosure to mitigate the effects of water vapor on the terahertz beam.^{6,7}

The terahertz radiation detector is an ion-implanted silicon-on-sapphire detection chip with the antenna geometry shown in Fig. 1(c). The 20- μm -wide antenna structure is embedded in a coplanar transmission line consisting of two parallel 10- μm -wide aluminum lines separated from each other by 30 μm . The electric field of the focused incoming terahertz radiation induces a transient bias voltage across the 5- μm gap between the two arms of this receiving antenna, which is directly connected to a low-noise current amplifier. The amplitude and time dependence of this transient voltage is obtained by measurement of the collected charge (average current) versus the time delay between the terahertz pulses and the colliding-pulse mode-locked laser detection pulses. These pulses in the 5-mW laser detection beam synchronously gate the receiver by driving (closing) the photoconductive switch defined by the 5- μm antenna gap. Simply speaking, the switch is closed by the photocarriers created by the 60-fs laser pulse; the switch then reopens in approximately 600 fs owing to the short carrier lifetime in ion-implanted silicon on sapphire.

The resulting system has demonstrated a signal-to-noise ratio of 5000, a time resolution faster than 200 fs, and a frequency range from 0.2 to more than 4 THz

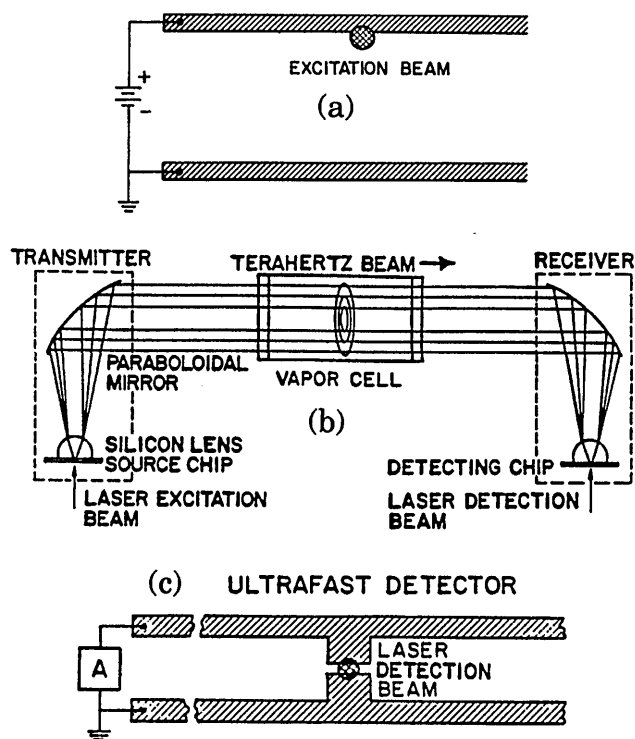


Fig. 1. (a) Optoelectronic configuration used to generate the freely propagating pulses of terahertz radiation. (b) Terahertz collimating and focusing optics together with a 22.5-cm-long vapor cell. (c) Receiving antenna geometry.

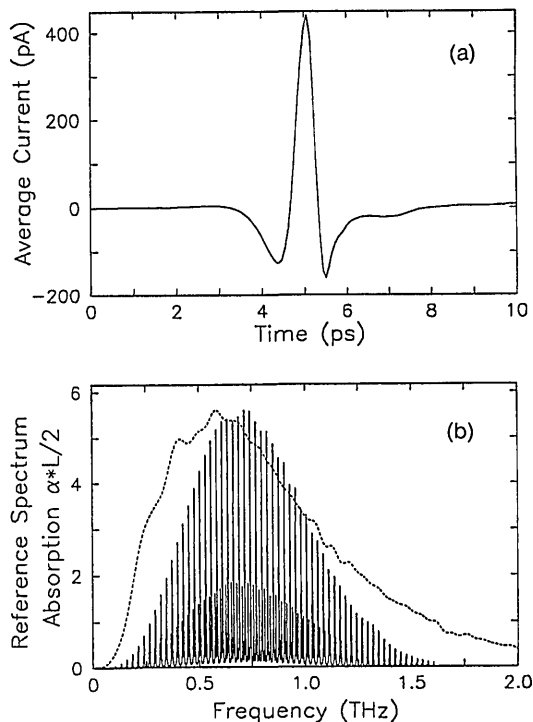


Fig. 2. (a) Measured terahertz reference pulse transmitted through an empty vapor cell. (b) Amplitude spectrum (dashed curve) of the reference pulse compared with the calculated methyl chloride absorption spectrum (including both chlorine isotopes) at 50 hPa.

(1 THz = $33.3 \text{ cm}^{-1} = 4.1 \text{ meV}$). Based on previous calculations⁹ and direct measurements, the average terahertz power incident upon the sample is 10 nW. Considering that the 0.4-ps terahertz pulses are separated by 10 ns, corresponding to the 100-MHz repetition rate, the peak power in the incident terahertz pulses is only 0.2 mW. Consequently the high signal-to-noise ratio for such low-power pulses shows that the detection of the terahertz radiation is extremely sensitive. In terms of average power, the sensitivity exceeds that of liquid-helium-cooled bolometers by more than 1000 times.¹⁹ In addition, because of the gated and coherent detection, the thermal background that plagues traditional measurements in this terahertz (far-infrared) range is observationally absent.

The most serious experimental problem limiting the accuracy of our measurements involves the relatively long-term changes in the laser pulses and the consequent changes in the input terahertz pulses. During an experiment we first measure the reference terahertz pulse (with no sample in place), then measure the terahertz pulse transmitted through the sample, and finally remeasure the reference pulse with the sample removed. This sequence is repeated several times to yield good statistics. Typically the amplitude spectral ratio of subsequent reference pulses varies by $\pm 5\%$ over the terahertz frequency spectrum. In the same manner the relative phase of subsequent reference pulses varies by ± 0.05 rad over the same spectrum.

A measured transmitted terahertz pulse is displayed in Fig. 2(a), where the FWHM is seen to be 0.45 ps. The system noise level is 0.5 pA. The corresponding ampli-

tude spectrum, obtained by a numerical Fourier transform of Fig. 2(a), is displayed as the dashed curve in Fig. 2(b). As is shown in Fig. 2(b), the entire ground-state rotational band of methyl chloride is overlapped by this amplitude spectrum.

3. MEASUREMENTS

A terahertz pulse propagating through methyl chloride vapor will be reshaped owing to the absorption and the dispersion of the vapor. These changes can be dramatic and are quantified by comparison of the transmitted pulse with the reference pulse (with no vapor in the cell). This is demonstrated by the measurements presented in Fig. 3. The reference pulse shown in Fig. 3(a) is the same pulse that is shown in Fig. 2(a) on an expanded time scale. When 10 hPa of methyl chloride vapor is added to the cell, the transmitted pulse changes to that shown in Fig. 3(b). Within the broad spectral range covered by the terahertz pulses the methyl chloride molecule has a manifold of pure rotational absorption lines [see Fig. 2(b)] that can be simultaneously excited in the impact approximation by the terahertz pulse. The molecules respond to this

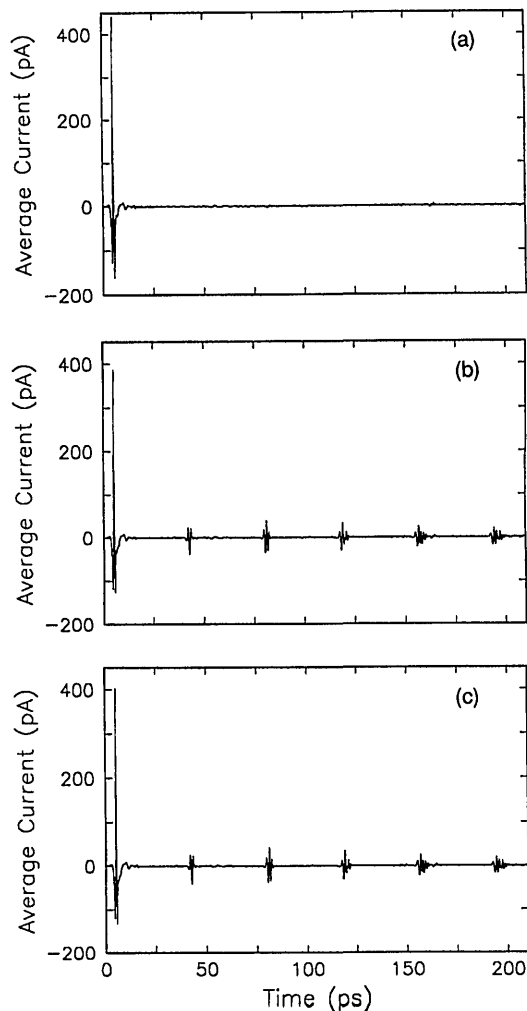


Fig. 3. (a) Terahertz reference pulse measured without vapor in the cell. (b) Measured transmitted terahertz pulse for 10 hPa of methyl chloride vapor. (c) Corresponding calculated transmitted terahertz pulse for 10 hPa of vapor.

excitation by reradiating an FID signal, which decays because of relaxation, interference, and propagation effects. Here one sees that the transmitted excitation pulse is followed by coherent transients emitted by the vapor. For this case the relative amplitude of the first transient is one tenth that of the excitation pulse, and well-defined subpicosecond coherent transients appear every 38 ps.

To understand these observations, it is essential to realize that the methyl chloride molecule is distinguished by a large number of uniformly spaced absorption lines, where to first order the frequency spacing between the lines is a constant. Consequently a periodic rephasing and dephasing of the entire ensemble of ~ 70 excited transitions occurs during the FID. After the initial excitation pulse, the sample emits a series of uniformly spaced subpicosecond terahertz pulses with a repetition rate of 26.3 GHz, equal to the frequency separation between adjacent lines and corresponding to a pulse separation of 38 ps. In conformity with our N_2O observations,³ we term these coherent transients terahertz commensurate echoes. The theoretical comparison with this measurement is shown in Fig. 3(c). The agreement between theory and experiment is excellent; every feature seen in the measurement is reproduced in the calculation.

We demonstrate the high performance of the optoelectronic terahertz system with its excellent signal-to-noise ratio and time resolution by looking more closely at selected individual echoes of the FID on a magnified time scale. Figure 4 displays the first, the third, and the fifth echoes emitted by the sample 38, 114, and 190 ps after the excitation pulse. To permit us to show these echoes more clearly and to suppress systematic reflections, the echoes shown are the difference between the 10-hPa transmitted pulse, Fig. 3(b), and the terahertz reference pulse of Fig. 3(a).

These echoes show a significant reshaping, which is due to several effects. First, methyl chloride has two chlorine isotopes, with their relative proportion given by the natural isotopic abundance. Consequently there are two independent and slightly shifted rotational spectra that manifest themselves in the time domain as two independent sets of echoes, gradually separating from each other with increasing time delay. In addition, the methyl chloride molecules show small deviations from the rigid-rotator model. As centrifugal forces increase the moment of inertia of the rotating molecule, the frequency spacing between adjacent rotational lines is not constant but decreases slightly with increasing rotational quantum number J . In the case of methyl chloride each rotational line further consists of a series of transitions associated with the quantum number K , representing the projection of the angular momentum on the molecular symmetry axis. Owing to the centrifugal stretching perpendicular to this axis, the degeneracy of the K transitions is abolished and an additional small line shift with increasing K is observed. Both of these effects cause an anharmonicity in the line spacing and thereby a gradual dephasing of the individual transitions, which is then seen as a change in the echo shape. By this dephasing the FID is washed out because of frequency shifts resulting from the motion of the molecules; by analogy to Doppler dephasing, in which a polarization is induced in the gas, we call this phenomenon centrifugal dephasing.^{3,4}

Finally, when the spectral peak absorption [see Fig. 2(b)] is much larger than unity, propagation effects can also strongly affect the observable pulse structure. Within an absorption line the gas is an optically thick sample with an attenuation as large as $500\times$. An individual line has a spectral width that is determined only by collisional broadening, whereas Doppler dephasing in this spectral range can be completely neglected. As long as the adjacent lines do not overlap and their widths increase linearly with pressure, the peak absorption is independent of the pressure. However, in the spectrum transmitted through an optically thick medium the absorption lines appear to be strongly broadened, which appears in the time domain as a faster decay of the echoes than is expected from collisional dephasing. Inherently combined with the absorption of the vapor is the dispersion, which in the vicinity of the rotational lines delays the different frequency components of the terahertz pulse differently and by this changes the observable pulse structure. The main contributions of the echo decay and reshaping, il-

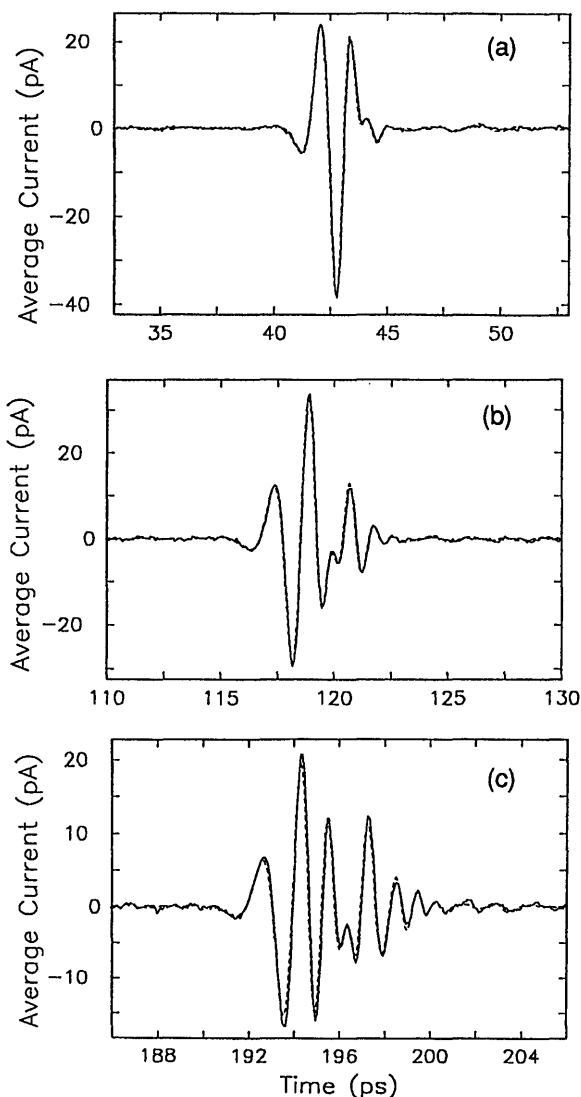


Fig. 4. Measurement (solid curves) and calculation (dashed curves) of the pulse shape of (a) the first, (b) the third, and (c) the fifth commensurate echoes on a magnified time scale for 10 hPa of methyl chloride vapor.

illustrated in Fig. 4, can be attributed to these propagation effects. Using the theoretical approach to be described below, we show the calculated pulse shapes of the coherent transients as the dashed curves in Figs. 4(a)–4(c); the dashed curves are nearly hidden by the solid curves (measurements). The excellent agreement is obtained when the echoes are fitted with rotational constants and centrifugal stretching constants of both isotopes, as is known from the literature.^{20,21}

Propagation effects that are due to dispersion become more significant with increasing pressure when a broader spectral range is affected by the phase shifts that are caused by the spectral lines. This is demonstrated by Fig. 5, which shows measurements for three different vapor pressures. For 10 hPa the transmitted excitation pulse has been only slightly attenuated and reshaped. The echo pulse train extends to beyond 1 ns, with initial echo amplitudes approximately 10% of that of the driving pulse. When the pressure is increased to 100 hPa, the amplitude of the transmitted pulse is reduced to approximately one third of its initial value, and the pulse is significantly reshaped. The relatively larger echo pulse train decays much more rapidly, and, compared with the 10-hPa results, the echoes are strongly reshaped. At 1000 hPa the transmitted driving pulse is severely attenuated and reshaped; only two echoes are easily observable.

As is shown in Fig. 6(a), at 1000 hPa the transmitted excitation pulse is completely reshaped owing to both the strong absorption and the dispersion of the vapor. The pulse has broken up and shows a fast beating on the leading edge, while the lower frequencies are shifted to the trailing edge. This produces a significant negative chirp over the pulse envelope because of the dominating negative dispersion in the vapor. The first echo has been stretched out and appears as a simple wave packet. Figure 6(b) shows the corresponding calculated pulse structure, which reproduces the measurement remarkably well in both pulse shape and amplitude for the exciting pulse as well as the echoes. This excellent agreement can be obtained only with van Vleck–Weisskopf line shapes for the rotational lines and the nonmonotonic J dependence for the collision broadening shown in Fig. 6(c), to be discussed in detail below.

4. THEORY

An accurate theoretical description and simulation of the measurements requires the solution of the coupled Maxwell–Bloch equations. However, under our low-power conditions we can assume a linear response of the sample to the excitation pulses. Then the Maxwell–Bloch equations reduce to those of linear dispersion theory.^{2–4} The interaction of the electric field with the medium can be described in the frequency domain by means of the complex propagation constant

$$k(\omega) = k_0 + \Delta k(\omega) + i\alpha(\omega)/2, \quad (1)$$

where $k_0 = \omega(n/c)$ is the nonresonant wave vector in the sample, and n the refractive index outside the material resonances. $\Delta k(\omega)$ describes the frequency-dependent phase change per unit length that is due to the resonant

interaction with the vapor, and $\alpha(\omega)$ the power absorption coefficient. The spectral field distribution $E(z, \omega)$ for a plane wave propagating in the z direction through the medium can then be written as

$$E(z, \omega) = E(0, \omega)\exp(ik_0z)\exp[i\Delta k(\omega)z]\exp[-\alpha(\omega)z/2], \quad (2)$$

and the corresponding propagating pulse, consisting of all the frequency components $E(z, \omega)$, is derived by the Fourier transformation of Eq. (2) as

$$E(z, t) = \int_{-\infty}^{\infty} E(0, \omega)\exp[-i(\omega t - k_0z)] \times \exp[i\Delta k(\omega)z]\exp\left[-\frac{1}{2}\alpha(\omega)z\right]d\omega, \quad (3)$$

where $E(0, \omega)$ is the spectral distribution of the input pulse given by the Fourier transform

$$E(0, \omega) = \frac{1}{2\pi} \int_{-\infty}^{\infty} E(0, t)\exp(i\omega t)dt. \quad (4)$$

With the spectral response of the vapor known, the propa-

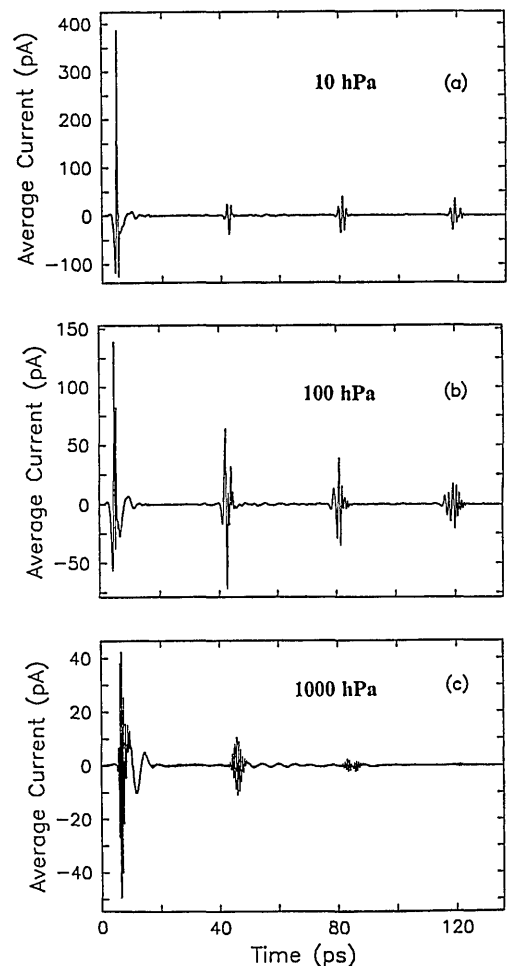


Fig. 5. (a) Measured transmitted terahertz pulse through 10 hPa of methyl chloride vapor. (b) Measured terahertz pulse through 100 hPa of vapor. (c) Measured terahertz pulse through 1000 hPa of vapor.

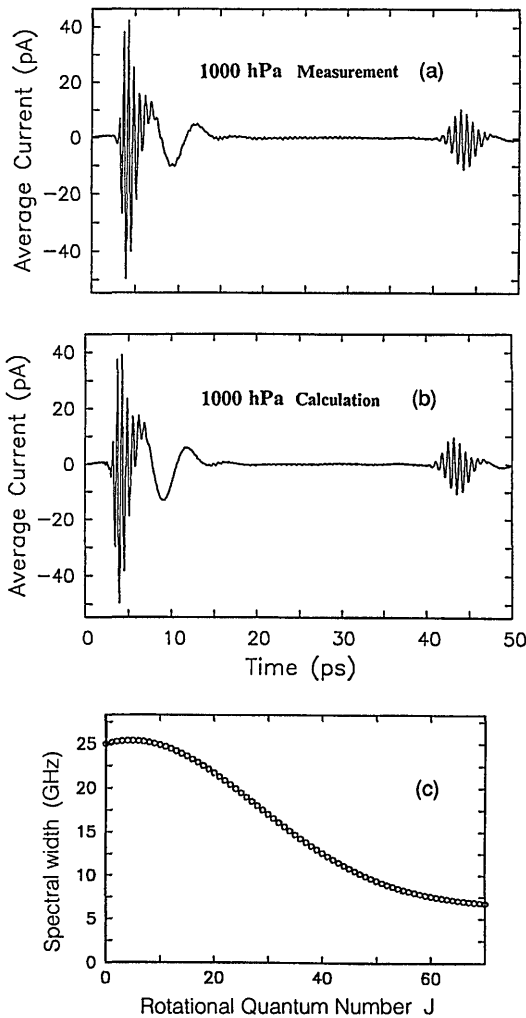


Fig. 6. (a) Measured transmitted terahertz pulse through 1000 hPa of methyl chloride vapor. (b) Calculated transmitted terahertz pulse through 1000 hPa vapor. (c) Experimentally determined J -dependent linewidth broadening for the vapor at 1000 hPa.

gation of the terahertz pulses through the vapor is derived by solution of Eq. (3), which rigorously satisfies the wave equation.

For methyl chloride, as a symmetric top molecule, each rotational state with total angular momentum P and rotational quantum number J consists of a manifold of $2J + 1$ sublevels associated with the projection of the angular momentum P_z on the molecular symmetry axis and indicated by the projection quantum number K . Excitation of the molecular vapor by the terahertz radiation induces transitions between pairs of J, K levels of the lowest vibrational state. Because for a symmetric top there exists no dipole moment perpendicular to the symmetry axis, no torque along this axis is associated with radiation, and therefore no angular momentum changes occur along this axis. Because of this selection rule, only transitions from J, K to $J + 1, K$ will be observed, and the absorption coefficient for such a transition, assuming unpolarized or unoriented molecules, can be calculated (for details see Ref. 22):

$$\alpha_{JK}(\omega) = \omega^2 C_{JK} G_A(\omega, \omega_{JK}), \quad (5)$$

with a van Vleck–Weisskopf line shape

$$G_A(\omega, \omega_{JK}) = \frac{\Delta\omega_J}{(\omega - \omega_{JK})^2 + (\Delta\omega_J/2)^2} + \frac{\Delta\omega_J}{(\omega + \omega_{JK})^2 + (\Delta\omega_J/2)^2} \quad (6)$$

and transition frequency

$$\frac{\omega_{JK}}{2\pi} = 2(J + 1)(B_V - D_{JK}K^2) - 4D_J(J + 1)^3. \quad (7)$$

The quantity C_{JK} is given by

$$C_{JK} = \frac{pf_0\mu^2 h B_V}{6nc\epsilon_0(kT)^3} \left(\frac{hA_V}{\pi kT} \right)^{1/2} \left(J + 1 - \frac{K^2}{J + 1} \right) \times \frac{S_W(I, K)}{4I^2 + 4I + 1} \times \exp[-h(B_V J(J + 1) + (A_V - B_V)K^2)/kT]. \quad (8)$$

Here, $\Delta\omega_J$ is the angular frequency linewidth (FWHM), assumed to be identical for different K transitions; B_V and A_V are the rotational constants of the vibrational state about the total angular momentum and symmetry axis; D_J and D_{JK} are the respective centrifugal stretching constants; p is the gas pressure; f_0 is the fraction of molecules in the lowest vibrational state; μ is the electric dipole moment, $S_W(I, K)$ is the statistical weight of a J, K level; I is the nuclear spin of a hydrogen atom; h is Planck's constant; kT is the thermal energy; c is the speed of light; and ϵ_0 is the vacuum permittivity.

For the change of the wave vector it is found that

$$\Delta k_{JK}(\omega) = C_{JK} \frac{2\omega\omega_{JK}^2}{\omega_{JK}^2 - \omega^2} G_N(\omega, \omega_{JK}), \quad (9)$$

where

$$G_N(\omega, \omega_{JK}) = 1 - \frac{\omega\Delta\omega_J^2}{8\omega_{JK}^2} \times \left[\frac{\omega + \omega_{JK}}{(\omega - \omega_{JK})^2 + (\Delta\omega_J/2)^2} + \frac{\omega - \omega_{JK}}{(\omega + \omega_{JK})^2 + (\Delta\omega_J/2)^2} \right]. \quad (10)$$

The absorption $\alpha(\omega)$ and dispersion $\Delta k(\omega)$ over the whole spectral range of the terahertz pulse are found by summation of Eqs. (5) and (9) over all transitions within this spectral width:

$$\alpha(\omega) = \sum_{J=0}^{\infty} \sum_{K=0}^J \alpha_{JK}(\omega), \quad (11)$$

$$\Delta k(\omega) = \sum_{J=0}^{\infty} \sum_{K=0}^J \Delta k_{JK}(\omega). \quad (12)$$

5. COMPARISON OF CALCULATIONS AND MEASUREMENTS

With the theoretical framework presented in the previous section, an analysis of a measurement can be performed by Fourier transformation of the measured pulse structure into the frequency domain and comparison of the result with the theoretical spectra, or the analysis can be done in the time domain by simulation of the pulse structure and direct comparison of the result with the measurement. In both cases the absorption and the dispersion of the vapor have to be calculated from Eqs. (5)–(12) with the known molecular constants.

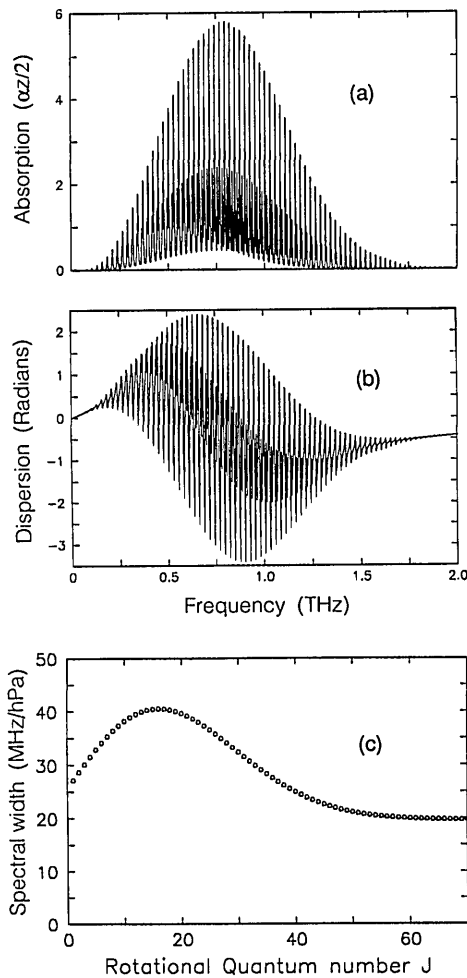


Fig. 7. Calculated (a) absorption and (b) dispersion in radians for 22.5 cm of 100 hPa of methyl chloride vapor. (c) The experimentally determined J -dependent linewidth used to calculate the absorption and the dispersion.

Here we present in more detail the analysis for the 100-hPa results. The theoretical amplitude absorption $\alpha L/2$ and phase change in radians ΔkL at 100 hPa, $L = 22.5$ cm, and $T = 294$ K are shown in Fig. 7. These spectra were calculated for methyl chloride as an isotopic mixture with the natural abundances of 75.4% for $\text{CH}_3^{35}\text{Cl}$ and 24.6% for $\text{CH}_3^{37}\text{Cl}$; the other parameters are $\mu = 1.869 \times 3.33 \times 10^{-30}$ A s m, $^{35}A_V = 156.05$ GHz, $^{37}A_V = 156.445$ GHz, $^{35}B_V = 13.292876$ GHz, $^{37}B_V = 13.088129$ GHz, $^{35}D_J = 18.089$ kHz, $^{37}D_J = 17.72$ kHz, $^{35}D_{JK} = 198.764$ kHz, and $^{37}D_{JK} = 193.67$ kHz (see Refs. 20 and 21). The statistical weight $S_W(I, K)$ with nuclear spin $I = 1/2$ for hydrogen and including the twofold degeneracy of levels with $|K| > 0$ becomes $S_W(I, K) = 4I^2 + 4I + 3 = 6$ for $K = 0$; $S_W(I, K) = 2(4I^2 + 4I + 3) = 12$ for $K = 3, 6, 9, \dots$; and $S_W(I, K) = 2(4I^2 + 4I) = 6$ for $K = 1, 2, 4, 5, 7, 8, 10, \dots$. At a temperature $T = 294$ K the fraction of molecules in the lowest vibrational state is $f_0 = 0.956$. The linewidth is given by the experimentally determined J -dependent function presented in Fig. 7(c). The details of the J dependence are discussed in Section 6.

The theoretical absorption and dispersion of the vapor can then be compared with the respective spectra derived

from the measurements by the method of terahertz time-domain spectroscopy.⁸ For this method two measured pulse shapes are needed, the transmitted pulse (reference pulse) with no vapor in the cell and the transmitted pulse (sample pulse) with vapor in the cell. This pair of pulses is shown in Figs. 8(a) and 8(b) for the 100-hPa measurement. From their numerical Fourier transforms and the relationship between their complex spectra given by Eq. (2), the amplitude absorption and the phase change can be obtained from the experimental data.

However, when the peak absorption is much larger than unity [see Fig. 7(a)] and frequencies at the band center are strongly attenuated ($\sim 500\times$) down to a level almost comparable with the noise, small amplitude fluctuations cause large uncertainties in the spectral absorption coefficient. The reason for this is the amplification of small fluctuations because of the logarithmic behavior close to zero.

Therefore, under conditions given here with a spectrally dense medium, we prefer to analyze the measurements by directly comparing them with a simulated pulse structure in the time domain. Our calculations are strictly numerical and are performed in the following manner. The measured reference pulse [Fig. 8(a)] is as

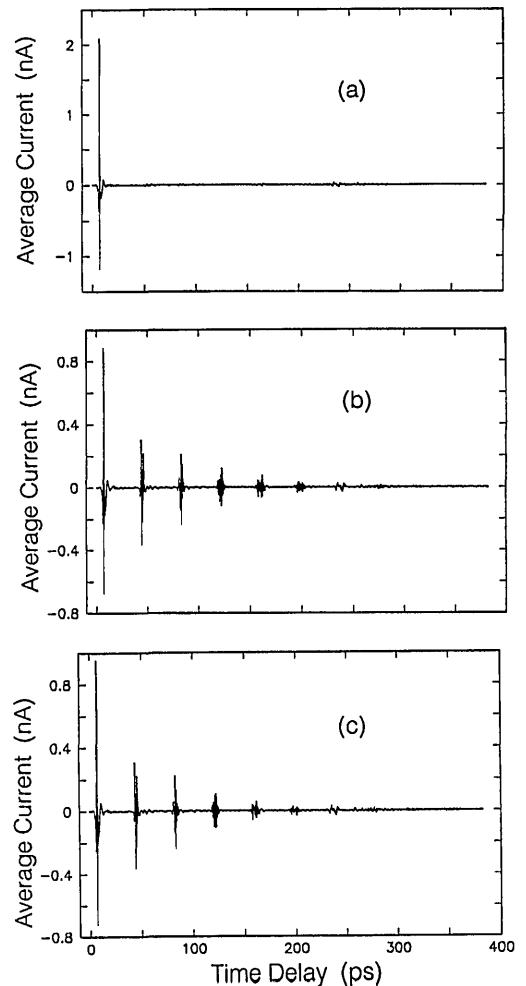


Fig. 8. (a) Reference pulse measured without vapor in the cell. (b) Measured transmitted terahertz pulse for 100 hPa of methyl chloride vapor. (c) Corresponding calculated transmitted terahertz pulse for 100 hPa of vapor.

sumed to be the input pulse to the vapor. Its numerical Fourier transform $E(0, \omega)$ is then multiplied by the theoretical amplitude absorption and dispersion, derived from Eqs. (5)–(12) and shown in Fig. 7. Finally, the inverse numerical Fourier transform of Eq. (3) is performed to yield the predicted output pulse. The final analysis is done by fitting of the simulated structure to the measurement by optimization of the parameters of the J -dependent linewidth and the molecular constants for the line spacing and anharmonicity.

The result of our numerical analysis is the predicted pulse train shown in Fig. 8(c). It reproduces the measurement in pulse shape and amplitude for the transmitted pulse as well as the commensurate echoes. This comparison is shown in more detail in Fig. 9 for the transmitted pulse [Fig. 9(a)], the first echo [Fig. 9(b)], the second echo [Fig. 9(c)], and the third echo [Fig. 9(d)]. The measurements shown as the solid curves are almost indistinguishable from the theory, shown as the dotted curves. For this excellent agreement it was essential to use the van Vleck–Weisskopf line shape together with the J -dependent collisional broadening given in Fig. 7(c). A fit of the rotational constants B_V and the centrifugal stretching parameters D_J and D_{JK} gave the values $^{35}B_V = 13.289(1)$ GHz, $^{37}B_V = 13.083(2)$ GHz, $^{35}D_J = 17.9(2)$ kHz, $^{37}D_J = 17.2(4)$ kHz, $^{35}D_{JK} = 150(30)$ kHz, and $^{37}D_{JK} = 90(40)$ kHz. The errors specified in parentheses (uncertainty of the last one or two digits) were estimated from the sensitivity of the parameters to the fitting procedure. It should be noted that the rotational constants derived from our analysis give slightly smaller values than those of Refs. 20 and 21. We explain this discrepancy as originating from pressure-induced line shifts of the rotational lines. Since our analysis does not distinguish between individual line shifts, the smaller rotational constants and stretching parameters compensate for an average pressure shift of the rotational spectrum to smaller frequencies.

To demonstrate conclusively the performance of the time-domain fitting procedure, we also provide the corresponding frequency-domain comparison for the 100-hPa measurements. However, owing to the sharp resonances in the rotational spectrum, a sensible comparison is possible only at an increased spectral resolution. Since the resolution is determined by the maximum time delay, the measured and the calculated pulse structures in Fig. 8, which consist of 8192 data points with a time interval of 0.04671 ps, were artificially expanded 8× by addition of a further 57,344 zeros separated by the same time interval. The n -fold extension of a data set by zeros at equally spaced time intervals is mathematically equivalent to an n -fold interpolation of the Fourier spectrum. A similar procedure is well known in Fourier-transform spectroscopy.²³

The amplitude spectra shown in Figs. 10(a) and 10(b) were obtained by transformation of the extended measured pulses of Figs. 8(a) and 8(b) and the calculated pulse structure of Fig. 8(c) into the frequency domain. The experimentally measured absorption $\alpha L/2$ obtained from the spectra of Fig. 10(a) is displayed on an expanded frequency scale in the series of spectra of Fig. 11. Here the dots indicate the results from the actual numerical Fourier transforms of Figs. 8(a) and 8(b), whereas

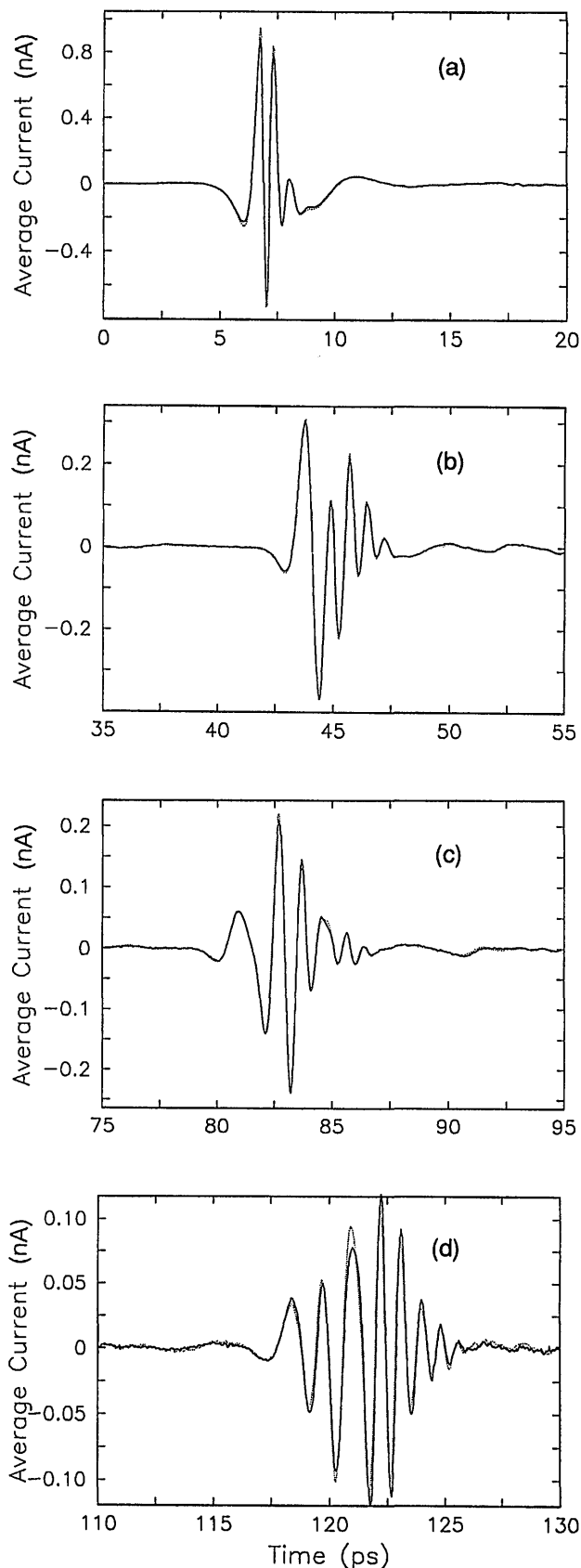


Fig. 9. Measurement of Fig. 8(b) (solid curves) and calculation of Fig. 8(c) (dotted curves) of the pulse shape of (a) the transmitted excitation pulse and (b) the first, (c) the second, and (d) the third commensurate echoes shown on a magnified time scale for 100 hPa of methyl chloride vapor.

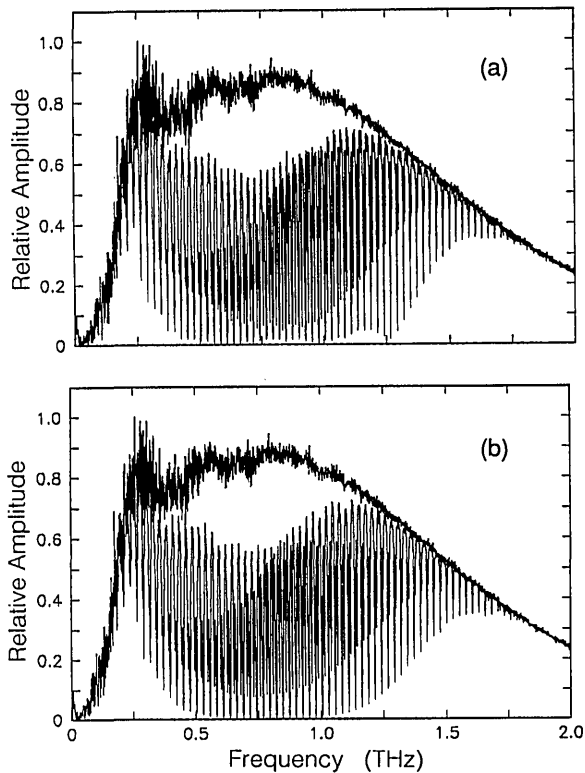


Fig. 10. (a) Fourier-transformed amplitude spectrum (upper curves) of the measured reference pulse of Fig. 8(a) compared with that of the pulse [Fig. 8(b)] transmitted through 22.5 cm of 100 hPa of methyl chloride vapor. (b) Spectrum of the reference pulse compared with that of the calculated pulse [Fig. 8(c)]. All pulses were extended 8× in the time domain by the addition of zeros before the numerical Fourier transform was taken.

the solid curves represent the absorption calculated from the extended data sets of Figs. 8(a) and 8(b). These results are compared with the calculated absorption (dotted curves) on the basis of the optimized molecular constants and J -dependent linewidths presented in Fig. 7(c). As can be seen, the agreement is exceptional and thereby assures us of the power and the accuracy of the time-domain analysis.

Using the self-pressure-broadening distribution of Fig. 7(c), we also get the excellent agreement between the calculation and the measurement for 10-hPa methyl chloride shown in Figs. 3 and 4. However, it should be noted that at this low pressure almost identical echo shapes are calculated with the assumption of a constant pressure-broadening parameter $C_w(300\text{ K}) = 32.4\text{ MHz/hPa}$ for all transitions. The reason for this is that at this low pressure and therefore narrow linewidths of the rotational transitions, with an experimentally realized delay time of 300 ps determining the experimental spectral resolution, it is not possible to distinguish between different linewidths.

6. SELF-PRESSURE BROADENING AND LINE-SHAPE INVESTIGATIONS

It is to be emphasized that the theory including the natural isotopic compound of methyl chloride, the centrifugal dephasing, and the propagation effects is in excellent agreement with the experiments. Therefore an

analysis of the measurements permits an accurate determination of the linewidth broadening that is due to the methyl chloride vapor pressure and by this the coherence relaxation time T_2 . This is true even under conditions when adjacent rotational transitions cannot be fully resolved, and a measurement in the frequency domain would be almost impossible. At the higher pressures propagation effects in an optically thick vapor considerably enhance the observation of the J -dependent pressure broadening and permit the line shape of the rotational transitions to be determined.

Our measurements cover a pressure range of more than 2 orders of magnitude, from 5 to 1000 hPa. At pressures below 100 hPa the individual linewidths increase linearly with pressure and can be expressed by the broadening parameter $C_J(T_0)$ of the distribution shown in Fig. 7(c) multiplied by the actual pressure. A change of the linewidth with temperature is assumed to vary with $C_J(T) = C_J(T_0)(T/T_0)^{-0.83}$ for a reference temperature of $T_0 = 300\text{ K}$.²⁴ The distribution of Fig. 7(c) can be represented by the empirically derived formula

$$C_J(T_0) = C_0 \left[r + (1 - r) \frac{J + A}{A} \exp(-J^2/\Delta^2) \right] \quad (13)$$

with a dependence on J similar to that for the absorption coefficient. This result takes into account that the part of the broadening that is due to resonant collisions is proportional to the number of molecules in the states involved. In Eq. (13) C_0 is the broadening parameter of the reference transition, $J = 0 \rightarrow J = 1$; r describes the remaining width at large J 's as the fraction of the initial width; A regulates the sharpness and the position of the maximum; and Δ determines the width as well as the maximum position of the distribution. With these parameters the linewidth variation of Fig. 7(c) is represented by $C_0 = 26.7\text{ MHz/hPa}$, $r = 0.725$, $A = 4.9$, and $\Delta = 24.5$.

As mentioned above, the experimentally realized delay time was not long enough to permit us to measure or confirm this linewidth distribution for pressures of 10 hPa or less. At these low pressures a reshaping of the echoes that is due to a changing linewidth can be observed only at delay times longer than 1 ns. However, the average broadening, and from this the average relaxation time T_2 , is determined quite accurately from the damping of the echoes. Since this decay of the echoes is also well represented by the distribution of Fig. 7(c), we assume the same dependence at this low pressure.

At pressures above 100 hPa, however, significantly changing distributions for the linewidth and a strong nonlinear broadening with vapor pressure can be observed. For example, at 1000-hPa, as a result of our time-domain fitting procedure, we obtain the distribution shown in Fig. 6(c), directly representing the actual linewidth of the rotational lines. To make the sensitivity of this fitting procedure clear, the strong influence of the J -dependent linewidth variation on the echo shape is demonstrated in Fig. 12 for the first echo of the 1000-hPa measurement. Figure 12(a) represents a calculation with a constant linewidth over the entire spectrum. The complete disagreement with the measurement, shown as

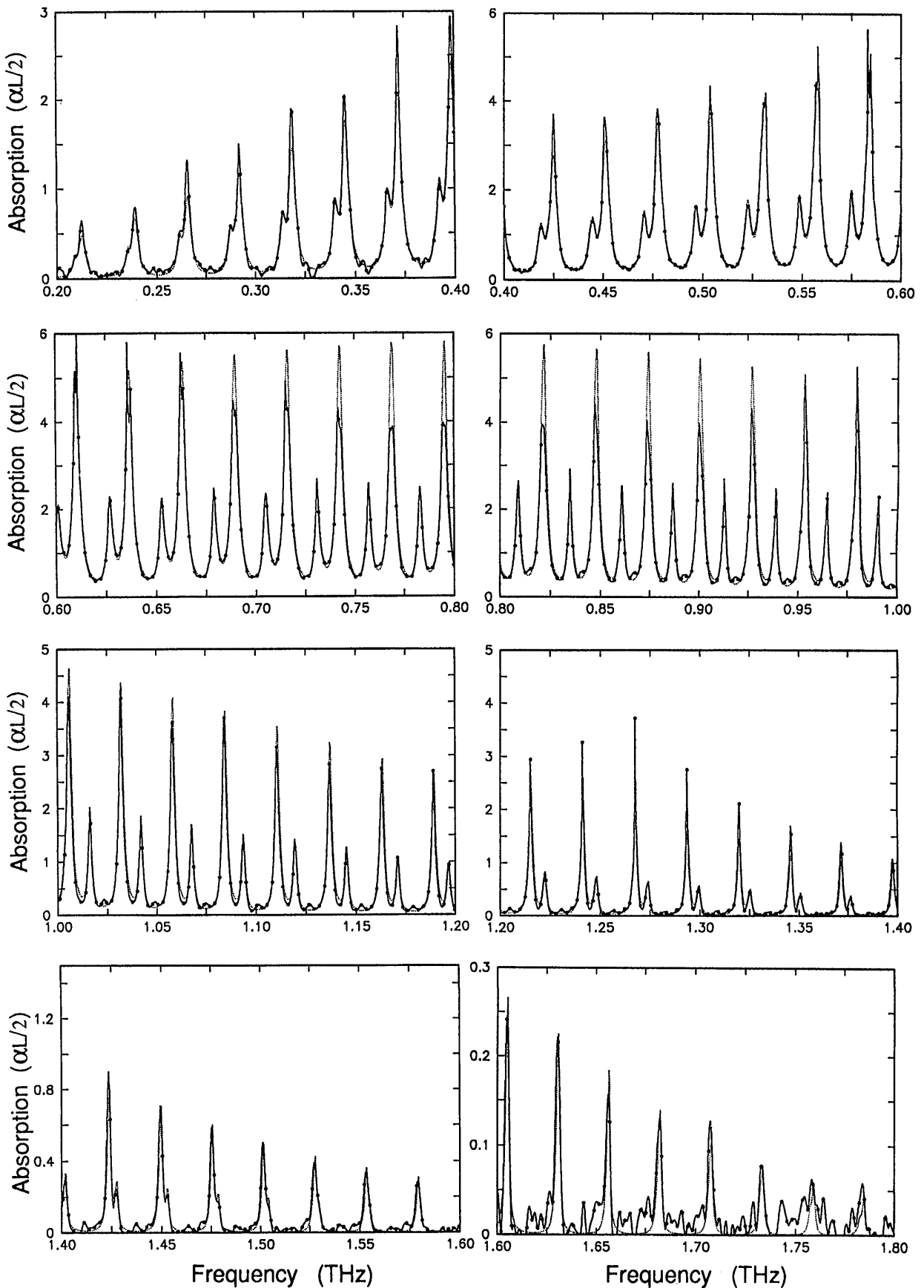


Fig. 11. Absorption $\alpha L/2$ for 22.5 cm of 100 hPa of methyl chloride vapor. The dots are obtained from the numerical transforms of Figs. 8(a) and 8(b). The solid curves are obtained from the numerical transforms of Figs. 8(a) and 8(b) after the pulses were extended $8\times$ in the time-domain by the addition of zeros. The dotted curves show the theoretical absorption of Fig. 7(a).

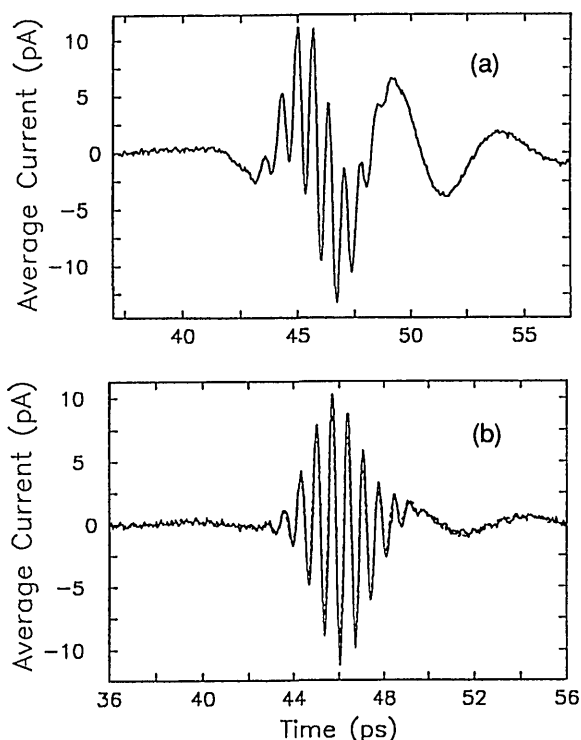


Fig. 12. (a) Calculated first echo pulse for 1000-hPa methyl chloride vapor with a constant linewidth for all the rotational transitions. (b) Measured first echo pulse for 1000 hPa (solid curve) compared with calculated echo pulse (dotted curve) with the J -dependent linewidth shown in Fig. 6(c).

the solid curve in Fig. 12(b), is striking. With the numerically determined J -dependent linewidth function of Fig. 6(c), the echo amplitude and the shape can be reproduced precisely, as is illustrated by the dashed curve in Fig. 12(b).

If propagation effects were neglected in the time-domain analysis of the pressure broadening, significantly larger linewidths would be obtained. This difference is due to the exponential dependency of the absorption and the dispersion. Under our experimental conditions the peak spectral absorption $\alpha_{\max}L/2$ cannot be assumed to be small compared with unity [see Figs. 2(b) and 7(a)]. At the line center, saturation effects cause an additional spectral broadening of the absorption lines shown in Fig. 10, and the exceptional dispersion of the rotational resonances [see Fig. 7(b)] contributes to an additional strong dephasing of the individual frequencies. In the time domain both these effects manifest themselves as a faster decay of the measured pulse train. As long as the linewidth is proportional to pressure and the individual lines are not overlapping, the absorption on line center is independent of pressure [see Eqs. (5) and (6)]. Then the only way to change the absorption and the dispersion is to change the length of the cell. With fixed T_2 (pressure) the apparent decay seen on the calculated FID pulse train becomes longer as the propagation length through the vapor becomes shorter. The decay approaches T_2 only for an optically thin sample, for which the remaining deviations are due to the centrifugal dephasing^{3,4} and the isotopic effect.

Perhaps the most surprising result of our analysis is that terahertz time-domain spectroscopy allows for

observations of small wing corrections to the line shape. Thus it is possible to differentiate clearly between different rotational line shapes at the high pressure of 1000 hPa, even though the individual rotational lines are strongly overlapping, as is illustrated by Fig. 13 for the calculated absorption and dispersion spectra. Since the transmitted excitation pulse reacts sensitively in its time shift and structure on the dispersion in the vapor, we find agreement only with the measured pulse structure for a van Vleck-Weisskopf line shape. This is demonstrated in Fig. 14(a) for the measurement (solid curve) in direct comparison with the simulation (dashed curve); a Lorentzian line shape with an absorptive profile almost indistinguishable from the van Vleck-Weisskopf line shape cannot fit the data [Fig. 14(b)]. The apparent time shift of the Lorentzian is not physically meaningful; only the details of the curve are pertinent.

A previous example of distinguishing between the Lorentzian and the van Vleck-Weisskopf line shapes for collision-broadened rotational lines relates to studies of the ammonia inversion spectrum (see, e.g., Refs. 22 and 25). These earlier measurements represent a sensitive test of pressure-broadening theory, and they demonstrate that deviations between the line shapes become significant when the lines are so broad that $\Delta\omega$ is comparable with the transition frequency ω_0 . In the ammonia inversion spectrum at 1 atm (760 Torr) the full width is $\Delta\omega = 2\pi \times 27$ GHz, and the transition frequency (at low pressures) is only $\omega_0 = 2\pi \times 23.4$ GHz. Then the ω^2 factor and the negative frequency resonance term in the

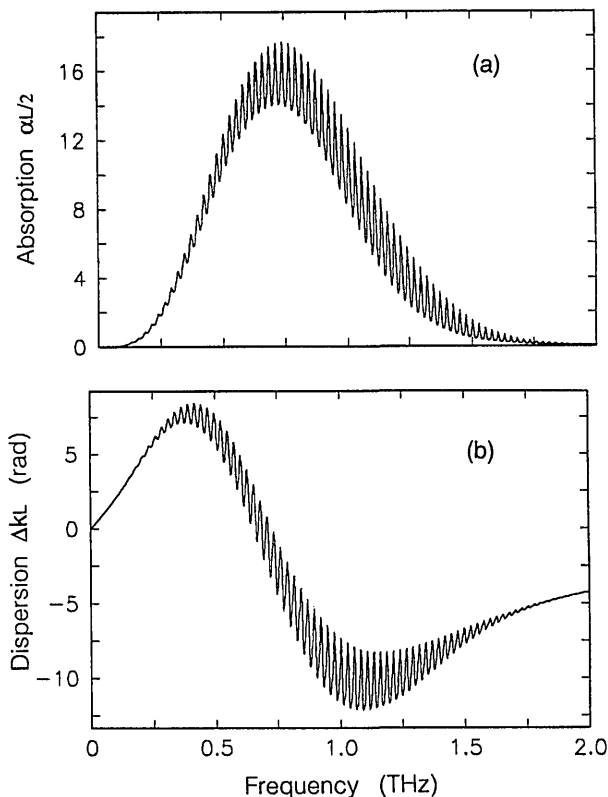


Fig. 13. (a) Calculated absorption and (b) dispersion in radians for 22.5 cm of 1000 hPa of methyl chloride vapor with the J -dependent linewidth of Fig. 6(c).

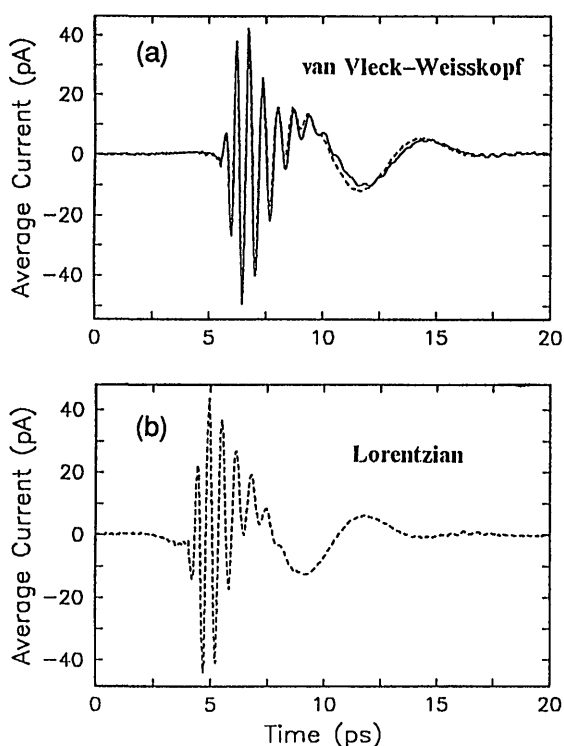


Fig. 14. (a) Measured transmitted terahertz pulse (solid curve) for 1000 hPa of methyl chloride vapor compared with calculated terahertz pulse (dashed curve) for the van Vleck-Weisskopf line shape. (b) Calculated terahertz pulse for 1000 hPa with the Lorentzian line shape.

van Vleck-Weisskopf line shape [see Eq. (6)] become apparent and permit discrimination from a Lorentzian.

In contrast to the above, the rotational linewidth of methyl chloride at 1 atm varies from 25 to 7 GHz (see Fig. 6), while the transition frequencies, which dominate in the spectrum, are well above 1 THz. Therefore $\Delta\omega_J \ll \omega_J$, and under these circumstances with classical absorption spectroscopy it is impossible to discriminate between the two absorption profiles, which differ by less than 10^{-3} . But our technique is also sensitive to the dispersion of the gas, and the dispersive curves of a Lorentzian or van Vleck-Weisskopf type can be well distinguished under these conditions. Their phase deviations accumulate over the whole rotational band and therefore contribute to a significant difference in the overall dispersion of the gas.

At 1 atm the first deviations from the van Vleck-Weisskopf shape are to be expected because of the failure of the impact collision model used in the van Vleck-Weisskopf theory, for which assumption of binary collisions no longer holds. An indication of this is that the pressure-broadening coefficient $\Delta\omega/p$ becomes smaller at higher pressures. This behavior has been observed in the ammonia measurements and also in our experiments. In the ammonia inversion spectrum discrepancies with the van Vleck-Weisskopf theory, as discussed by Townes and Schawlow,²² are seen as a shift of the transition frequency and the decreasing pressure-broadening coefficient.

If, however, these parameters are used as empirical values, the experimental absorption curves can be fitted

quite well by a van Vleck-Weisskopf line shape. Bleaney and Loubser²⁵ show such fits to their experimental data at various pressures from 10 to 4560 Torr. For pressures of 2 or more atmospheres (1 atm = 760 Torr), ω_0 has to be set to zero, and the van Vleck-Weisskopf theory is reduced to the Debye theory. A shift of the transition frequency with increasing pressure for a line shape that is otherwise the same as given by van Vleck and Weisskopf can be derived from the more complex theory of Anderson,²⁶ but it should be noticed that Anderson's theory also assumes collisions to be short compared with the interval between the collisions (i.e., binary collisions).

Our simulations using the van Vleck-Weisskopf line shape and fitting the rotational constants as well as the linewidths gives the excellent agreement demonstrated above. The results also show a small pressure-induced frequency shift of the rotational constants, which, however, is less than 10^{-3} (see Section 5).

Deviations from the predicted line shape caused by infringements of the impact theory in general can also be observed in the more distant wings of a line, where the shape is governed to an increasing extent by the specific perturbations (depending on the interaction forces) of the energy levels during collision rather than merely by the frequency of collisions. In the experiments presented here such effects were not resolved. However, in an ongoing more-detailed study of pressure broadening, in which we are using a terahertz-beam system with a bandwidth extending to 5 THz, the far-wing absorption on the high-frequency side of the rotational band is being measured out to more than 200 linewidths from the resonances. For this case observations of small wing corrections in the shape are obtained.

With increasing vapor pressure a gradual shift of the entire measured pulse structure to longer delay times is observed because of the increase of the non-resonant refractive index n with vapor density, e.g., a pressure of 1013 hPa causes a time shift of 586 fs. Using the reference pulse, taken without methyl chloride vapor in the cell, as input for the simulated pulse structure and fitting the theoretical pulse to measurements at higher pressures, we evaluate an index change of $\Delta n = 7.2 \times 10^{-7} \text{ hPa}^{-1}$.

7. CONCLUSION

Using the technique of terahertz time-domain spectroscopy, we have experimentally and theoretically studied methyl chloride vapor. After excitation by a subpicosecond pulse of terahertz electromagnetic radiation, the vapor sample was observed to emit a train of subpicosecond terahertz pulses. The decaying train of subpicosecond pulses, separated from one another by 38 ps, extended to beyond 1 ns, and within the train the individual pulse shapes gradually changed. Because the experiments were performed under conditions for which the vapor behaves as a spectrally thick sample, propagation effects considerably influenced these observations. The reshaping was found to result from the anharmonicity in the line spacing caused by centrifugal stretching, the absorptive and the dispersive propagation effects, varying linewidth broadening over the rotational spectrum, and the isotopic composition of the vapor. Because the

experiments were performed in the low-intensity limit of the coupled Maxwell–Bloch equations, a linear dispersion theory analysis was used to compare theory with the observations. The resulting excellent agreement between theory and experiment permitted the determination of the frequency separation between the individual methyl chloride lines, the centrifugal stretching constants, and the coherent relaxation time T_2 as a function of vapor pressure, even for the case of strongly overlapping lines. Our observations indicate that the individual rotational transitions have van Vleck–Weisskopf line shapes with a strong nonmonotonic J dependence for the collision-broadening coefficient.

ACKNOWLEDGMENTS

H. Harde thanks IBM for hospitality and the Deutsche Forschungsgemeinschaft for financial support.

*Permanent address, Oklahoma State University, Stillwater, Oklahoma 74078.

REFERENCES AND NOTES

- See, e.g., A. Abragam, *The Principles of Nuclear Magnetism* (Oxford U. Press, New York, 1961).
- See, e.g., L. Allen, and J. H. Eberly, *Optical Resonance and Two Level-Atoms* (Wiley, New York, 1975).
- H. Harde, S. Keiding, and D. Grischkowsky, "Terahertz commensurate echoes: periodic rephasing of molecular transitions in free-induction decay," *Phys. Rev. Lett.* **66**, 1834 (1991).
- H. Harde and D. Grischkowsky, "Coherent transients excited by subpicosecond pulses of terahertz radiation," *J. Opt. Soc. Am. B* **8**, 1642 (1991).
- M. van Exter, Ch. Fattinger, and D. Grischkowsky, "High brightness terahertz beams characterized with an ultrafast detector," *Appl. Phys. Lett.* **55**, 337 (1989).
- M. van Exter, Ch. Fattinger, and D. Grischkowsky, "Terahertz time-domain spectroscopy of water vapor," *Opt. Lett.* **14**, 1128 (1989).
- M. van Exter, Ch. Fattinger, and D. Grischkowsky, "Time-domain far-infrared spectroscopy of water vapor and direct measurement of collisional relaxation times," in *Laser Spectroscopy IX—Proceedings of the Ninth International Conference on Laser Spectroscopy*, M. S. Feld, J. E. Thomas, and A. Mooradian, eds. (Academic, San Diego, Calif., 1989).
- D. Grischkowsky, S. Keiding, M. van Exter, and Ch. Fattinger, "Far-infrared time-domain spectroscopy with terahertz beams of dielectrics and semiconductors," *J. Opt. Soc. Am. B* **7**, 2006 (1990), and subsequent measurements in our laboratory to 6 THz.
- M. van Exter and D. Grischkowsky, "Characterization of an optoelectronic terahertz beam system," *IEEE Trans. Microwave Theory Tech.* **38**, 1684 (1990).
- R. G. Brewer, "Coherent optical spectroscopy," in *Frontiers in Laser Spectroscopy*, R. Balian, S. Haroche, and S. Liberman, eds. (North-Holland, Amsterdam, 1977), p. 341.
- R. L. Shoemaker, "Coherent transient infrared spectroscopy," in *Laser and Coherence Spectroscopy*, J. I. Steinfeld, ed. (Plenum, New York, 1978), p. 197.
- M. Rosatzin, D. Suter, W. Lange, and J. Mlynek, "Phase and amplitude variations of optically induced spin transients," *J. Opt. Soc. Am. B* **7**, 1231 (1990).
- K. L. Foster, S. Stenholm, and R. G. Brewer, "Interference pulses in optical free induction decay," *Phys. Rev. A* **10**, 2318 (1974).
- M. Woerner, A. Seilmeier, and W. Kaiser, "Reshaping of infrared picosecond pulses after passage through atmospheric CO₂," *Opt. Lett.* **14**, 636 (1989).
- J. P. Heritage, T. K. Gustafson, and C. H. Lin, "Observation of coherent transient birefringence in CS₂ vapor," *Phys. Rev. Lett.* **34**, 1299 (1975).
- K. Bratengeier, H.-G. Purucker, and A. Laubereau, "Free induction decay of inhomogeneously broadened lines," *Opt. Commun.* **70**, 393 (1989).
- N. Katzenellenbogen and D. Grischkowsky, "Efficient generation of 380 fs pulses of terahertz radiation by ultrafast laser pulse excitation of a biased metal–semiconductor interface," *Appl. Phys. Lett.* **58**, 222 (1991).
- S. E. Ralph and D. Grischkowsky, "Trap-enhanced electric fields in semi-insulators: the role of electrical and optical carrier injection," *Appl. Phys. Lett.* **59**, 1972 (1991).
- C. Johnson, F. J. Low, and A. W. Davidson, "Germanium and germanium-diamond bolometers operated at 4.2 K, 2.0 K, 1.2 K, 0.3 K and 0.1 K," *Opt. Eng.* **19**, 255 (1980).
- A. Dubrulle, D. Boucher, J. Burie, and J. Demaison, "The high resolution rotational spectrum of methyl chloride—the spin–rotation and nuclear magnetic shielding tensors," *Chem. Phys. Lett.* **45**, 559 (1977).
- P. Jensen, S. Brodersen, and G. Guelachvili, "Determination of A_0 for CH₃³⁵Cl and CH₃³⁷Cl from the $\sqrt{4}$ infrared and Raman bands," *J. Mol. Spectrosc.* **88**, 378 (1981).
- C. H. Townes and A. L. Schawlow, *Microwave Spectroscopy* (Dover, New York, 1975).
- P. R. Griffiths, *Chemical Infrared Fourier Transform Spectroscopy* (Wiley, New York, 1975).
- W. Wensink, H. A. Dijkerman, and R. W. Parsons, "The broadening and shifting of the $J = 0 \rightarrow 1$ line of CH₃Cl by the foreign gases CH₃Br, OCS and CO₂," *Phys. Lett.* **50A**, 331 (1974).
- B. Bleaney and J. H. N. Loubser, "The inversion spectra of NH₃, CH₃Cl and CH₃Br at high pressure," *Proc. Phys. Soc.* **63A**, 483 (1950).
- P. W. Anderson, "Pressure broadening in the microwave and infra-red regions," *Phys. Rev.* **76**, 647 (1949).